

# Simulating Damage Mechanics of Electromigration and Thermomigration

Shidong Li  
Mohd F. Abdulhamid  
Cemal Basaran

Electronic Packaging Laboratory  
State University of New York at Buffalo,  
102 Ketter Hall, Buffalo, NY, 14260  
cjb@buffalo.edu

Electromigration (EM) and thermomigration (TM) are processes of mass transport which are critical reliability issues for next generation nanoelectronics and power electronics. The purpose of this project is to develop a computational tool for simulating damage mechanics of EM and TM and their interaction. In this paper, a model for EM and TM processes is proposed and has been implemented in a general purpose finite-element code. The governing equations utilized for the model include mass conservation, force equilibrium, heat transfer and electricity conduction. A damage evolution model based on thermodynamics is introduced to evaluate the degradation in solder joints subjected to high current densities and high temperature gradients. The simulation results are compared with experimental data to validate the model.

**Keywords:** Electromigration, thermomigration, nanoelectronics packaging, thermodynamics, damage mechanics

## 1. Introduction

The next generation ultra-large-scale integration (ULSI) electronics and solder joints are expected to carry very high current densities and operate under very high temperature gradients. Under high current density, metals and alloys undergo electromigration (EM) and thermomigration (TM). However, there is no commercially available computational mechanics software that can analyze an electronic package's degradation due to high current density and high temperature gradients. The purpose of this study is the development of such a computational mechanics simulation tool.

Because of their low melting temperature and high diffusivity, solder joints are the weakest link in the electronic package. Solder joints failure is a process in which many mechanisms work together. The major factors include mass transportation, electrical conduction, heat transfer and the corresponding mechanical stresses. In this study, a model is developed and implemented by Finite Element Method (FEM) that accounts for all these mechanisms.

High current density and large temperature gradients create four distinct diffusion driving forces.

1. Electrical current field forces include two driving mechanisms. One is the electrostatic force of the electric field. The other is the so-called electron wind force as originally suggested by Skaupy [1]. The electron wind force refers to the effect of the momentum exchange between the scattered moving free electrons and ionic atoms. This momentum exchange happens because of the scattering of free valence electrons. Scattered electrons collide with metal atoms and gently push them in the direction of electron flow [2, 3].
2. Thermal gradient is one of the strongest driving forces. Joule heating generated by high electricity current density is highly localized and consequently results in a large thermal gradient in the medium, which leads to TM. The physical explanation behind TM is not well understood. However, recent literature shows that TM could play a significant role in EM-induced failure [4–8].
3. Stress gradient is another driving force of mass transport. There is a strong interaction between the stress gradient and the other driving forces. Stress gradient can counteract or enhance the migration

process [9–17]. However, in the absence of an external stress gradient, as the mass moves from the hot side to the cold side, compression on the cold side and tension on the hot side develops. This counters the thermal gradient and electrical field induced forces.

4. The atomic vacancy concentration gradient, which is usually small at the beginning compared to the former two items [18], increases significantly as the mass migration progresses the vacancy concentration gradient between the hot and cold sides.

## 2. Governing Equations and Discretization

Electromigration is a diffusion-controlled mass transport process. It is governed by the mass conservation equation. The vacancy diffusion is governed by the vacancy conservation equation. The mechanical equilibrium is governed by the force equilibrium equation. Heat transfer is governed by Fourier's law. Finally, the electric field in a conducting material is governed by Maxwell's equation of conservation of charge.

In the following presentation of the model development, the governing equations will first be introduced and discretized for FEM application. Tang and Basaran's [19] viscoplastic model for solder alloys is then introduced, which can simulate the viscoplastic behavior under a high current density well.

### 2.1 Mass Conservation

Electromigration is governed by the following vacancy conservation equation, which is equivalent to the mass conservation equation:

$$C_{V0} \frac{\partial c}{\partial t} + \nabla \cdot \mathbf{q} - G = 0 \quad (1)$$

where  $C_{V0}$  is the equilibrium vacancy concentration in the absence of stress field,  $c (= C_V/C_{V0})$  is the normalized vacancy concentration,  $C_V$  is vacancy concentration,  $t$  is time and  $\mathbf{q}$  is vacancy flux [18, 20, 21]. Vacancy flux is defined:

$$\mathbf{q} = -D_V C_{V0} \left( \nabla c + \frac{Z^* e}{kT} (\nabla \phi) c + \frac{cf\Omega}{kT} \nabla \sigma^{sp} + \frac{c}{kT^2} Q^* \nabla T \right) \quad (2)$$

where  $D_V$  is vacancy diffusivity,  $Z^*$  is vacancy effective charge number,  $e$  is electron charge,  $\phi$  is electrical potential,  $\mathbf{j}$  is current density (vector),  $f$  is vacancy relaxation ra-

tio (ratio of atomic volume to the volume of a vacancy),  $\Omega$  is atomic volume,  $k$  is Boltzmann's constant,  $T$  is absolute temperature,  $\sigma^{sp} (= \text{trace}(\sigma_{ij})/3)$  is the spherical part of stress tensor,  $Q^*$  is heat of transport (the isothermal heat transmitted by moving the atom in the process of jumping a lattice site, less the intrinsic enthalpy) and  $G$  is vacancy generation/annihilation rate, defined:

$$G = -C_{V0} \frac{c - \exp\left(\frac{(1-f)\Omega\sigma^{sp}}{kT}\right)}{\tau_s} \quad (3)$$

where  $\tau_s$  is characteristic vacancy generation/annihilation time.

### 2.2 Finite Element Method Implementation

Implementing Equation (1) using the method of weighted residuals, we can write:

$$\int_V \delta c \left( C_{V0} \frac{\partial c}{\partial t} + \nabla \cdot \mathbf{q} - G \right) dV = 0. \quad (4)$$

By taking the derivative with respect to normalized vacancy concentration  $c$ , we can write

$$[K_{cc}^1] = \int_V N^T \frac{1}{\Delta t} N dV \quad (5)$$

$$[K_{cc}^2] = \int_V \frac{\partial N^T}{\partial x} D_V \times \left[ \frac{\partial}{\partial x} + \frac{f\Omega}{kT_{n+1}} \nabla \sigma_{n+1}^{sp} + \frac{Q^* \nabla T_{n+1}}{kT_{n+1}^2} + \frac{Z^* e}{kT_{n+1}} \nabla \phi_{n+1} + \frac{c_{n+1} f \Omega}{kT_{n+1}} \frac{\partial \nabla \sigma_{n+1}^{sp}}{\partial c_{n+1}} \right] N dV \quad (6)$$

$$[K_{cc}^3] = \int_V -N^T \times \left[ \frac{\frac{(1-f)\Omega}{kT_{n+1}} \exp\left(\frac{(1-f)\Omega\sigma_{n+1}^{sp}}{kT_{n+1}}\right) \frac{\partial \sigma_{n+1}^{sp}}{\partial c_{n+1}} - 1}{\tau_s}} \right] N dV. \quad (7)$$

We have

$$[K_{cc}^{cc}] = [K_{cc}^1] + [K_{cc}^2] + [K_{cc}^3]. \quad (8)$$

By taking the derivative with respect to temperature  $T$ ,

$$[K_{cT}^1] = - \int_V N^T \frac{1}{\tau_s} \exp\left(\frac{(1-f)\Omega\sigma_{n+1}^{sp}}{kT_{n+1}}\right) \times \frac{(1-f)\Omega}{kT_{n+1}} \left(\frac{\partial\sigma_{n+1}^{sp}}{\partial T_{n+1}} - \frac{\sigma_{n+1}^{sp}}{T_{n+1}}\right) NdV \quad (9)$$

$$[K_{cT}^2] = \int_V \frac{\partial N^T}{\partial x} D_V \frac{cf\Omega}{kT_{n+1}} \cdot \left(\frac{\partial\nabla\sigma_{n+1}^{sp}}{\partial T_{n+1}} - \frac{\nabla\sigma_{n+1}^{sp}}{T_{n+1}}\right) NdV \quad (10)$$

$$[K_{cT}^3] = \int_V \frac{\partial N^T}{\partial x} D_V \frac{cQ^*}{kT_{n+1}^2} \times \left(\frac{\partial}{\partial x} - 2\frac{\nabla T_{n+1}}{T_{n+1}}\right) NdV \quad (11)$$

$$[K_{cT}^4] = - \int_V \frac{\partial N^T}{\partial x} D_V \frac{Z^*e}{kT_{n+1}} \times \nabla\varphi_{n+1}c_{n+1} \frac{1}{T_{n+1}} NdV. \quad (12)$$

We have

$$\begin{aligned} [K_{n+1}^{cT}] &= [K_{cT}^1] + [K_{cT}^2] + [K_{cT}^3] + [K_{cT}^4] \\ &= - \int_V N^T \frac{1}{\tau_s} \exp\left(\frac{(1-f)\Omega\sigma_{n+1}^{sp}}{kT_{n+1}}\right) \\ &\quad \times \frac{(1-f)\Omega}{kT_{n+1}} \left(\frac{\partial\sigma_{n+1}^{sp}}{\partial T_{n+1}} - \frac{\sigma_{n+1}^{sp}}{T_{n+1}}\right) NdV \\ &\quad + \int_V \frac{\partial N^T}{\partial x} D_V \left[\frac{cf\Omega}{kT_{n+1}} \left(\frac{\partial\nabla\sigma_{n+1}^{sp}}{\partial T_{n+1}} - \frac{\nabla\sigma_{n+1}^{sp}}{T_{n+1}}\right) \right. \\ &\quad \left. + \frac{cQ^*}{kT_{n+1}^2} \left(\frac{\partial}{\partial x} - 2\frac{\nabla T_{n+1}}{T_{n+1}}\right) \right. \\ &\quad \left. - \frac{Z^*e}{kT_{n+1}} \nabla\varphi_{n+1}c_{n+1} \frac{1}{T_{n+1}}\right] NdV. \quad (13) \end{aligned}$$

By taking the derivative with respect to displacement  $u$ ,

$$[K_{cu}^1] = \int_V D_V \frac{\partial N^T}{\partial x} \frac{c_{n+1}f\Omega}{kT} \frac{\partial}{\partial x} \left(\frac{\partial\sigma_{n+1}^{sp}}{\partial\varepsilon_{n+1}}\right) BdV \quad (14)$$

$$[K_{cu}^2] = - \int_V N^T \frac{(1-f)\Omega}{kT_{n+1}} e \frac{\frac{\partial\sigma_{n+1}^{sp}}{\partial\varepsilon_{n+1}}}{\tau_s} BdV \quad (15)$$

$$[K_{n+1}^{cu}] = [K_{cu}^1] + [K_{cu}^2], \quad (16)$$

where  $B$  is the strain-displacement matrix.

### 2.3 Force Equilibrium

Note that

$$\sigma_{ij,j} = 0. \quad (17)$$

The incremental stress-strain constitutive model is established as

$$\sigma = \mathbb{C}(\varepsilon, \dot{\varepsilon}) \cdot (\varepsilon - \varepsilon_D - \varepsilon_{TE}) \quad (18)$$

where  $\varepsilon$  is the total strain,  $\varepsilon_D$  is strain due to electromigration and thermomigration,  $\varepsilon_{TE}$  is strain due to thermal expansion and  $\mathbb{C}(\varepsilon, \dot{\varepsilon})$  is the tangential viscoplastic strain-stress constitutive tensor.

Integrating the weak form of Equation (17), we obtain

$$\int_V \delta u \sigma_{ij,j} dV = 0. \quad (19)$$

By taking the first-order derivative with respect to  $u$ , we obtain

$$[K_{n+1}^{uu}] = \int_V B^T \mathbb{C}(\varepsilon, \dot{\varepsilon}) BdV. \quad (20)$$

By taking the derivative with respect to  $c$ , we have

$$[K_{n+1}^{uc}] = \int_V B^T \otimes \frac{\partial\sigma_{n+1}^{sp}}{\partial c_{n+1}} \otimes NdV. \quad (21)$$

By taking the derivative with respect to  $T$ , we have

$$[K_{n+1}^{uT}] = \int_V B^T \otimes \frac{\partial\sigma_{n+1}^{sp}}{\partial T_{n+1}} \otimes NdV. \quad (22)$$

### 2.4 Heat Transfer

Heat transfer is described by

$$\rho C_p \frac{\partial T}{\partial t} - \nabla(k_h \nabla T) - \rho Q = 0 \quad (23)$$

where  $\rho$  is density of the material,  $C_p$  is specific heat and  $k_h$  is the coefficient of heat transfer.  $Q$  is the heat generated within the body, which can be expressed

$$Q = Q_J + Q_P + Q_V \quad (24)$$

where  $Q_J$  is heat due to Joule heating,  $Q_P$  is the heat generated by plastic deformation and  $Q_V$  is the heat due to vacancy flux.

$Q_J$  can be written

$$Q_J = \frac{1}{\Delta t} \int_{\Delta t} Q_J(t) dt. \quad (25)$$

Using linear assumption, Equation (25) can be expanded as

$$Q_J = E_{n+1} \frac{1}{R} E_{n+1} - E_{n+1} \frac{1}{R} \Delta E_{n+1} + \frac{1}{3} \Delta E_{n+1} \frac{1}{R} \Delta E_{n+1} \quad (26)$$

$R$  is electrical resistance, where  $E$  is the electrical field intensity, defined as

$$E = -\frac{\partial \phi}{\partial x}. \quad (27)$$

By Ohm's law, the flow of electrical current is described as

$$J = \frac{E}{R} = -\frac{1}{R} \frac{\partial \phi}{\partial x}. \quad (28)$$

$Q_P$  is the heat generated by plastic deformation at step  $n + 1$  and can be written

$$Q_P = \sigma_{n+1} : \dot{\epsilon}_{n+1}^{pl} \quad (29)$$

where  $\dot{\epsilon}^{pl}$  is the plastic strain rate.

$Q_V$  can be expressed

$$Q_V = \mathbf{q} : F_k \quad (30)$$

where  $\mathbf{q}$  is vacancy flux as in Equation (2) and  $F_k$  is the effective driving force which is defined

$$F_k = - \left( Z^* e \nabla \phi + f \Omega \nabla \sigma^{sp} + \frac{Q^*}{T} \nabla T + \frac{kT}{c} \nabla c \right). \quad (31)$$

Equation (30) can be expanded at step  $n + 1$  as

$$Q_V = D_V C_V \frac{c_{n+1}}{kT_{n+1}} \left( \frac{kT_{n+1}}{c_{n+1}} \nabla c_{n+1} + Z^* e \nabla \phi_{n+1} + f \Omega \nabla \sigma_{n+1}^{sp} + \frac{Q^* \nabla T_{n+1}}{T_{n+1}} \right)^2 \quad (32)$$

and by using the weighted residuals method, Equation (23) can be rewritten as

$$\int_V \delta T \left( \rho C_p \frac{\partial T}{\partial t} - \nabla (k_h \nabla T) - \rho Q \right) dV = 0. \quad (33)$$

By taking the derivative with respect to  $T$  we obtain

$$[C_{n+1}^{TT}] = \int_V N^T \frac{C_p}{\Delta t} N dV \quad (34)$$

$$[K_{TT}^1] = \int_V \frac{\partial N^T}{\partial x} \frac{k_h}{\rho} \frac{\partial N}{\partial x} dV \quad (35)$$

$$[K_{TT}^2] = \int_V N^T \frac{\partial Q_{n+1}^J}{\partial T_{n+1}} N dV = \int_V N^T \left( -\frac{1}{R^2} \frac{\partial R}{\partial T_{n+1}} \right) \left( \frac{\partial \phi_{n+1}}{\partial x} \frac{\partial \phi_{n+1}}{\partial x} - \frac{\partial \phi_{n+1}}{\partial x} \frac{\partial \Delta \phi_{n+1}}{\partial x} + \frac{1}{3} \frac{\partial \Delta \phi_{n+1}}{\partial x} \frac{\partial \Delta \phi_{n+1}}{\partial x} \right) N dV \quad (36)$$

$$[K_{TT}^3] = \int_V N^T \frac{\partial Q_{n+1}^V}{\partial T_{n+1}} N dV = \int_V N^T \frac{D_V C_V c_{n+1}}{k} \times \frac{\left[ \begin{array}{l} \frac{k \nabla c_{n+1}}{c_{n+1}} N \\ + f \Omega \frac{\partial \sigma_{n+1}^{sp}}{\partial T_{n+1}} N \\ + \frac{Q^*}{T_{n+1}} \frac{\partial N}{\partial x} \\ - \frac{Q^* \nabla T_{n+1}}{T_{n+1}^2} N \end{array} \right]}{T_{n+1}^2} dV \quad (37)$$

and we can write

$$[K_{n+1}^{TTT}] = [C_{n+1}^{TT}] + [K_{TT}^1] + [K_{TT}^2] + [K_{TT}^3]. \quad (38)$$

By taking the derivative with respect to  $c$ , we obtain

$$[K_{n+1}^{Tc}] = - \int_V N^T \frac{\partial Q_{n+1}^V}{\partial c_{n+1}} N dV = - \int_V \frac{D_V C_V}{k T_{n+1}} \left[ (F_{n+1}^k)^2 N - 2 F_{n+1}^k c_{n+1} \times \left( f \Omega \frac{\partial \sigma_{n+1}^{sp}}{\partial c_{n+1}} \frac{\partial N}{\partial x} + \frac{k T_{n+1}}{c_{n+1}^2} \times \left( c_{n+1} \frac{\partial N}{\partial x} - \nabla c N \right) \right) \right] dV. \quad (39)$$

By taking the derivative with respect to  $u$ , we obtain

$$[K_{n+1}^{Tu}] = - \int_V N^T \frac{\partial Q_{n+1}^P}{\partial u_{n+1}} N dV = - \int_V N^T \times \left( \frac{\partial \sigma_{n+1}^{dev}}{\partial \varepsilon_{n+1}} + \frac{1}{\Delta t} \frac{\partial \Delta \varepsilon_{n+1}^P}{\partial \varepsilon_{n+1}} \right) B dV. \quad (40)$$

By taking the derivative with respect to  $\varphi$ , we obtain

$$[K_{n+1}^{T\varphi}] = - \int_V N^T \frac{\partial Q_{n+1}^J}{\partial \varphi_{n+1}} N dV = \int_V N^T \left( J - \frac{1}{3} \Delta J \right) \frac{\partial N}{\partial x} dV. \quad (41)$$

### 2.5 Electrical Conduction Governing Equations

The electrical field in a conducting material is governed by Maxwell's equation of conservation of charge. Assuming steady-state direct current and no internal volumetric current source, the equation reduces to

$$\int_S J n dS = 0 \quad (42)$$

where  $S$  is the surface of a control volume,  $n$  is the outward normal to  $S$  and  $J$  is the electrical current density defined in Equation (28).

The divergence theorem is used to convert the surface integral into a volume integral:

$$\int_V \frac{\partial}{\partial x} J dV = 0. \quad (43)$$

The equivalent weak form is obtained by introducing an arbitrary, variational, electrical potential field  $\delta\varphi$  and integrating over the volume:

$$\int_V \delta\varphi \frac{\partial}{\partial x} J dV = 0. \quad (44)$$

By taking the derivative with respect to  $\varphi$  we have

$$[K_{n+1}^{\varphi\varphi}] = \int_V \frac{\partial N^T}{\partial x} \frac{1}{R} \frac{\partial N}{\partial x} dV. \quad (45)$$

By taking the derivative with respect to  $T$  we obtain

$$[K_{n+1}^{\varphi T}] = \int_V \frac{\partial N^T}{\partial x} E \left( \frac{1}{R^2} \frac{\partial R}{\partial T_{n+1}} \right) N dV. \quad (46)$$

Finally, we obtain the Jacobian matrix:

$$[K_{n+1}] = \begin{bmatrix} [K_{n+1}^{uu}] & [K_{n+1}^{uc}] & [K_{n+1}^{uT}] & 0 \\ [K_{n+1}^{cu}] & [K_{n+1}^{cc}] & [K_{n+1}^{cT}] & 0 \\ [K_{n+1}^{Tu}] & [K_{n+1}^{Tc}] & [K_{n+1}^{TT}] & [K_{n+1}^{T\varphi}] \\ 0 & 0 & [K_{n+1}^{\varphi T}] & [K_{n+1}^{\varphi\varphi}] \end{bmatrix}. \quad (47)$$

### 3. Viscoplastic Material Model

The complexity of this problem comes from the coupling terms between different governing equations. Because of the nonlinear behavior of the material, a local integration scheme is also needed. The return mapping algorithm is utilized for integration of material model. The strain-stress constitutive model in the absence of viscosity is established as

$$\boldsymbol{\sigma} = \mathbb{C}(\boldsymbol{\varepsilon}_{\text{total}} - \boldsymbol{\varepsilon}_{\text{visoplastic}} - \boldsymbol{\varepsilon}_{\text{diffusion}} - \boldsymbol{\varepsilon}_{\text{thermal}}) \quad (48)$$

where

$$\mathbb{C} = \kappa \mathbf{1} \otimes \mathbf{1} + 2\mu \left( \mathbf{I} - \frac{1}{3} \mathbf{1} \otimes \mathbf{1} \right),$$

$\kappa$  is bulk modulus,  $\mu$  is shear modulus,

$$\mathbf{I} = \begin{bmatrix} 1 & 0 & 0 & 0 & 0 & 0 \\ 0 & 1 & 0 & 0 & 0 & 0 \\ 0 & 0 & 1 & 0 & 0 & 0 \\ 0 & 0 & 0 & 0 & 0 & 0 \\ 0 & 0 & 0 & 0 & 0 & 0 \\ 0 & 0 & 0 & 0 & 0 & 0 \end{bmatrix} \quad \text{and} \quad \mathbf{1} = \begin{bmatrix} 1 \\ 1 \\ 1 \\ 0 \\ 0 \\ 0 \end{bmatrix}.$$

The tensor trace of  $\boldsymbol{\varepsilon}_{\text{diffusion}}$  can be described by the following [21]:

$$\frac{\partial \boldsymbol{\varepsilon}_{\text{diffusion}}^{\text{trace}}}{\partial t} = \Omega C_{V0} (f \nabla \mathbf{q} + f' G) \quad (49)$$

where  $f' = 1 - f$ .

Using Equation (1), we can transform Equation (49) into

$$\begin{aligned} \frac{\partial \boldsymbol{\varepsilon}_{\text{diffusion}}^{\text{trace}}}{\partial t} &= \Omega C_{V0} \left( G - f \frac{\partial c}{\partial t} \right) \\ &= \Omega C_{V0} \left( \frac{\exp\left(\frac{(1-f)\Omega\sigma_{sp}}{kT}\right) - c}{\tau_s} - f \frac{\partial c}{\partial t} \right). \end{aligned} \quad (50)$$

Establish a trial state by assuming elastic behavior at current step  $n + 1$ , i.e.

$$\mathbf{s}_{n+1}^{\text{trial}} = 2\mu \left( \mathbf{I} - \frac{1}{3} \mathbf{1} \otimes \mathbf{1} \right) (\boldsymbol{\varepsilon}_{n+1}^{\text{dev}} - \boldsymbol{\varepsilon}_{n+1}^{\text{vp}}) \quad (51)$$

where  $\mathbf{s}$  is the deviatoric stress.

Taking into account kinematic hardening, the effective stress can be defined as

$$\boldsymbol{\xi}_{n+1}^{\text{trial}} = \mathbf{s}_{n+1}^{\text{trial}} - \mathbf{X}_n \quad (52)$$

where  $\mathbf{X}_n$  is the back stress tensor that defines kinematic hardening, given by

$$\frac{\partial \mathbf{X}}{\partial t} = \gamma \frac{2}{3} H'(\alpha) \frac{\boldsymbol{\xi}}{\|\boldsymbol{\xi}\|} \quad (53)$$

where  $H'(\alpha)$  is the kinematic hardening modulus and  $\alpha$  is equivalent plastic strain given by

$$\alpha = \int \sqrt{\frac{2}{3} \dot{\varepsilon}_{ij}^p \dot{\varepsilon}_{ij}^p} dt.$$

Yield function is defined by

$$f_{n+1} = \|\boldsymbol{\xi}_{n+1}\| - \sqrt{\frac{2}{3}} K(\alpha_n) \quad (54)$$

and trial yield function is defined by

$$f_{n+1}^{\text{trial}} = \|\boldsymbol{\xi}_{n+1}^{\text{trial}}\| - \sqrt{\frac{2}{3}} K(\alpha_n). \quad (55)$$

The viscoplastic flow rule is given by

$$\dot{\varepsilon}_{ij}^{\text{vp}} = \frac{AD_0Eb}{k\theta} \left( \frac{\langle F \rangle}{E} \right)^n \left( \frac{b}{d} \right)^p e^{-Q/R\theta} \frac{\partial \mathbf{F}}{\partial \sigma_{ij}}. \quad (56)$$

The stress can then be updated as

$$\boldsymbol{\sigma}_{n+1} = \mathbf{s}_{n+1} + \frac{1}{3} Tr(\boldsymbol{\sigma}_{n+1}) \mathbf{I} = \mathbf{s}_{n+1} + \sigma_{n+1}^{\text{sp}} \mathbf{I} \quad (57)$$

where  $\sigma_{n+1}^{\text{sp}}$  is defined as

$$\begin{aligned} \sigma_{n+1}^{\text{sp}} &= \sigma_n^{\text{sp}} + \kappa \left( Tr(\Delta \boldsymbol{\varepsilon}_{n+1}^{\text{total}}) \right. \\ &\quad \left. - Tr(\Delta \boldsymbol{\varepsilon}_{n+1}^{\text{diffusion}}) - Tr(\Delta \boldsymbol{\varepsilon}_{n+1}^{\text{thermal}}) \right). \end{aligned} \quad (58)$$

After simple manipulation, the contribution of the displacement to the Jacobian can be expressed by Equations (59) and (65). For  $i, j = 1, 2, 3$ :

$$\begin{aligned} \mathbb{k}_{ij} &= \frac{\kappa^2 (\Omega \Delta t \Xi)^2}{1 + 3\kappa \Omega \Delta t \Xi} \mathbb{k}'_{ij} - \kappa \Omega \Delta t \Xi \sum_{j=1}^3 \mathbb{k}'_{ij} \\ &\quad + \frac{\kappa}{1 + 3\kappa \Omega \Delta t \Xi} + \mathbb{k}_{ij} \end{aligned} \quad (59)$$

where

$$\mathbb{k}'_{\text{total}} = \sum_{i,j=1}^3 \mathbb{k}'_{\text{total}}{}^{ij} \quad (60)$$

$$\Xi = \frac{C_{V0} \frac{(1-f)\Omega}{kT} \exp\left(\frac{(1-f)\Omega \sigma_{n+1}^{\text{sp}}}{kT}\right)}{3\tau_s} \quad (61)$$

$$\begin{aligned} \mathbb{k}'_{n+1} &= 2\mu \left( \theta_{n+1} \left( \mathbf{I} - \frac{1}{3} \mathbf{1} \otimes \mathbf{1} \right) \right. \\ &\quad \left. + \bar{\theta}_{n+1} \mathbf{n}_{n+1} \otimes \mathbf{n}_{n+1} \right) \end{aligned} \quad (62)$$

with

$$\theta_{n+1} = 1 + \frac{\Delta \gamma 2\mu}{\|\boldsymbol{\xi}_{n+1}^{Tr}\|} \quad (63)$$

and

$$\begin{aligned} \bar{\theta}_{n+1} &= \left( \frac{1}{2\mu} \frac{\partial \Theta}{\partial \Delta \gamma} + \frac{K'(\alpha_{n+1}) + H'(\alpha_{n+1})}{3\mu} \right)^{-1} \\ &\quad - \frac{\Delta \gamma 2\mu}{\|\boldsymbol{\xi}_{n+1}^{Tr}\|}. \end{aligned} \quad (64)$$

For  $i, j = 4, 5, 6$ ,

$$\mathbb{k}_{n+1}^{ij} = \mathbb{k}'_{n+1}{}^{ij}. \quad (65)$$

From Equation (58) we can obtain

$$\frac{\partial \sigma_{n+1}}{\partial c_{n+1}} = -\kappa C_{V0} \Omega \delta_{ij} \left( \Delta t \frac{\partial G}{\partial c_{n+1}} - \frac{f \partial \Delta c_{n+1}}{\partial c_{n+1}} \right). \quad (66)$$

By inserting Equation (3) into Equation (66), we obtain

$$\begin{aligned} \frac{\partial \sigma_{n+1}}{\partial c_{n+1}} &= -\delta_{ij} \kappa \Omega C_{V0} \left( \frac{\Delta t}{\tau_s} + f \right) \\ &\quad + \delta_{ij} \kappa \Omega C_{V0} \Delta t \frac{(1-f)\Omega}{3kT_{n+1}\tau_s} \\ &\quad \times \exp\left(\frac{(1-f)\Omega \sigma_{n+1}^{\text{sp}}}{kT_{n+1}}\right) \\ &\quad \times \left( \sum_{i,j=1}^3 \delta_{ij} \frac{\partial \sigma_{n+1}^{ij}}{\partial c_{n+1}} \right). \end{aligned} \quad (67)$$

By solving the above equations, we obtain

$$\frac{\partial \sigma_{n+1}^{ij}}{\partial c_{n+1}} = \frac{\delta_{ij} \kappa \Omega C_{V0} \left( \frac{\Delta t}{\tau_s} + f \right)}{1 + 3\kappa \Omega C_{V0} \Delta t \frac{(1-f)\Omega}{3kT_{n+1}\tau_s} \exp\left(\frac{(1-f)\Omega \sigma_{n+1}^{sp}}{kT_{n+1}}\right)}. \quad (68)$$

By taking the derivative of Equation (58) with respect to  $T$ , and considering that

$$\frac{\partial \Delta T_{n+1}}{\partial T_{n+1}} = \frac{\partial (T_{n+1} - T_n)}{\partial T_{n+1}} = 1,$$

we can obtain

$$\begin{aligned} \frac{\partial \sigma_{n+1}^{sp}}{\partial T_{n+1}} &= -\kappa \Omega C_{V0} \frac{\Delta t}{\tau_s} \exp\left(\frac{(1-f)\Omega \sigma_{n+1}^{sp}}{kT_{n+1}}\right) \\ &\times \frac{(1-f)\Omega}{k} \left( \frac{1}{T_{n+1}} \frac{\partial \sigma_{n+1}^{sp}}{\partial T_{n+1}} - \frac{\sigma_{n+1}^{sp}}{T_{n+1}^2} \right) \\ &- 3\alpha\kappa. \end{aligned} \quad (69)$$

Solving this, we can write

$$\frac{\partial \sigma_{n+1}^{sp}}{\partial T_{n+1}} = \frac{\mathcal{H} \sigma_{n+1}^{sp}}{T_{n+1}^2 + \mathcal{H} T_{n+1}}. \quad (70)$$

Where

$$\mathcal{H} = \kappa \Omega C_{V0} \frac{\Delta t}{\tau_s} \exp\left(\frac{(1-f)\Omega \sigma_{n+1}^{sp}}{kT_{n+1}}\right) \frac{(1-f)\Omega}{k}. \quad (71)$$

#### 4. Thermodynamics-based Damage Mechanics Model

It has been shown by Basaran et al. [18, 22–25] that the damage in solids can be quantified by entropy production, which can be accomplished by tracking the change in disorder parameter in Boltzmann's equation. A variable  $D$  is defined as the ratio of the change in disorder parameters to the original reference state, as follows:

$$D = D_{cr} \left( 1 - \exp\left(\frac{s_0}{N_0 k} - \frac{s}{N_0 k}\right) \right). \quad (72)$$

where  $D_{cr}$  is the critical damage parameter used to define the failure of a specific application,  $s_0$  and  $s$  are the entropy of a unit volume at the reference and current state, respectively, and  $k$  is Boltzmann's constant.  $N_0$  is Avogadro's number.  $D_{cr}$  is also used in a function form to correlate entropy production with specific mechanical property degradation. The  $D$  value starts at zero and reaches  $D = D_{cr}$  at the final stage.

Expanding the exponent term in this equation to Taylor's series, and ignoring the higher order terms, yields the simplification:

$$D = D_{cr} \left[ 1 - \exp\left(\frac{-\Delta s}{N_0 k}\right) \right]. \quad (73)$$

The entropy produced in an irreversible process caused by TM can be expressed as

$$\begin{aligned} \Delta s &= \int_{t_0}^t \left( \frac{1}{T^2} c \nabla T : \nabla T + \frac{C_V D_V}{k T^2} F_k \right. \\ &: \left. F_k + \frac{1}{T} \sigma : \dot{\epsilon}^P \right) dt. \end{aligned} \quad (74)$$

The damage evolution formula can be derived by substituting Equation (74) into Equation (73):

$$\begin{aligned} D &= D_{cr} \left[ 1 - \exp \right. \\ &\times \left. \left( \frac{-\int_{t_0}^t \left( \frac{1}{T^2} c \nabla T : \nabla T + \frac{C_V D_V}{k T^2} F_k : F_k + \frac{1}{T} \sigma : \dot{\epsilon}^P \right) dt}{N_0 k} \right) \right]. \end{aligned} \quad (75)$$

Using principles of continuum damage mechanics, Equation (75) can be implemented in the elasticity stress-strain relations [26]:

$$d\sigma = (1 - D) C d\epsilon. \quad (76)$$

Making use of the strain equivalence principle, the hardening rule and viscoplastic rule finally have the forms

$$F = \|\mathbf{S} - \mathbf{X}\| - (1 - D) \sqrt{\frac{2}{3}} \bar{\sigma}(\alpha) \quad (77)$$

and

$$\dot{\mathbf{X}} = (1 - D) (c_1 \dot{\epsilon}_{ij}^{vp} - c_2 \mathbf{X} \dot{\alpha}). \quad (78)$$

The model described in the preceding sections was implemented using general purpose Finite Element Method (FEM) code a commercial FEM software ABAQUS, by means of user-defined element User Element interface provided (UEL) by ABAQUS and user-defined material model User MATerial interface (UMAT).

#### 5. Testing and Finite Element Simulation

The test vehicle used in this study is a 27 mm × 27 mm × 0.97 mm flip-chip package, which involves a 7.62 mm × 7.62 mm × 0.74 mm silicon die interconnected to a 0.3 mm thick two-layer substrate with 720 solder bumps shown in Figures 1 and 2. The diameter of the solder bump is 140 μm while the standoff is 100 μm. The aluminum trace interconnect on the die is 1 μm thick and the copper trace on the Printed Wiring Board (PWB) substrate is 15 μm thick. The solder alloy is 95.5 Sn-4 Ag-0.5 Cu (SnAgCu solder Alloy (SAC) 405 in wt %) which is bonded with 96.5 Sn-3 Ag-0.5 Cu (SAC 305) presolder.

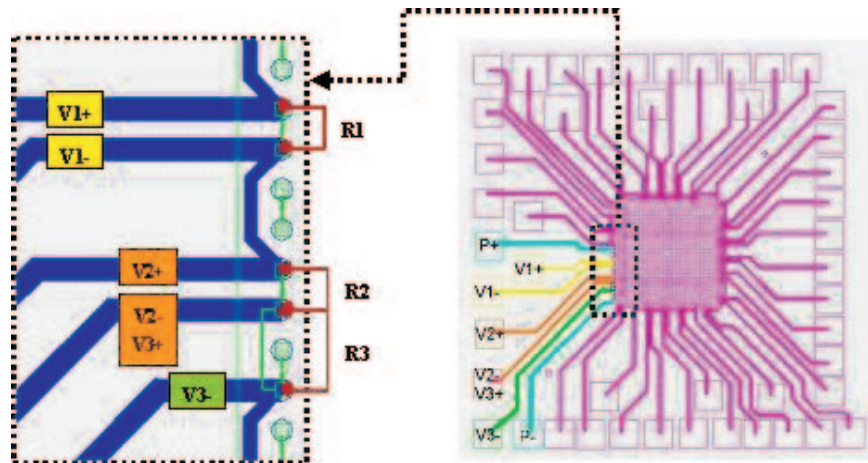


Figure 1. Circuit and solder joints on flip-chip test vehicle

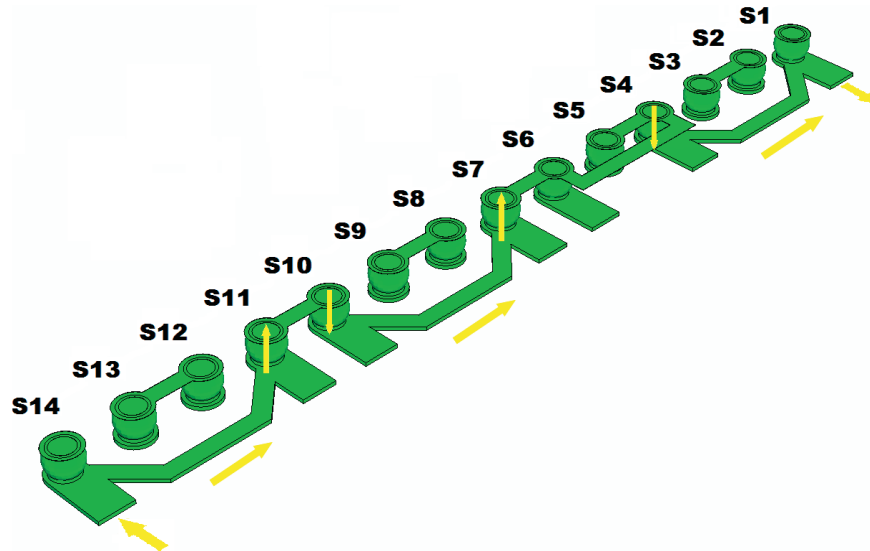


Figure 2. Electrified daisy chain and direction of current

The layout of circuits and solder joints on the flip-chip test vehicle is shown in Figure 1. Only a single daisy chain at the edge of the die on the encompassed region is electrified with a constant electric current of 2.5 A. The configuration of the daisy chain and the path of the current and solder joint numbers are shown in Figure 2. During testing, the daisy chain (Figure 2) was connected to a constant DC power supply with the positive terminal connected to V1+ and the negative terminal to P-, as shown in Figure 1.

A series of specimens were tested in the thermal chamber with ambient temperatures of -20, -30, -40 and -50°C. The purpose of running the experiments in low

temperatures is to be able to run very large current densities.

Failure is defined as when the system electrical resistance exceeds 1 ohm in all stressing cases, in order to avoid melting of solder joint, consequently destroying the microstructure.

Thermal properties for the materials used in analysis are listed in Table 1 [27]. In damage evolution analysis, the molar heat flux of SAC 405 alloy is 22.16 kJ mole<sup>-1</sup> [28] and the temperature dependent diffusivity is [29]:

$$D_V = 272 \exp\left(\frac{-48953}{RT}\right) \times 10^8 \text{ (m}^2\text{s}^{-1}\text{)}.$$

**Table 1.** Thermal material property

	SAC 405	Copper	Aluminum
Density ( $\text{kg } \mu\text{m}^{-3}$ )	$7.39 \times 10^{-15}$	$8.92 \times 10^{-15}$	$2.70 \times 10^{-15}$
Thermal conductivity ( $\text{W } \mu\text{m}^{-1} \text{K}^{-1}$ )	$57.3 \times 10^{-6}$	$4.16 \times 10^{-4}$	$2.38 \times 10^{-4}$
Electrical conductivity ( $\text{O}^{-1} \mu\text{m}^{-1}$ )	6.67	59.17	38.17
Specific heat ( $\text{J kg}^{-1} \text{K}^{-1}$ )	200	385	902

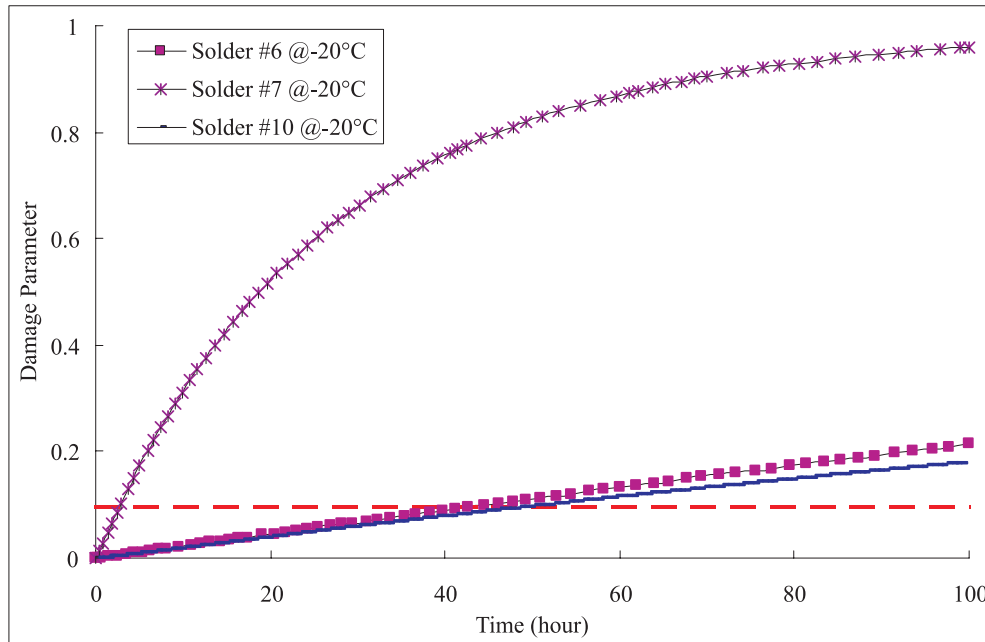


**Figure 3.** Damage evolution of three solders at  $-20^{\circ}\text{C}$

The rest of the material properties used in this paper are taken from Lin [30].

### 6. Discussion of Results

After a preliminary coupled thermal electrical analysis using ABAQUS standard, it is concluded that solder #7 and solder #10 are those with the maximum current density in the entire model. Solder #6 has the highest temperature at die side, as its top is located at a right angle junction of the Al trace which acts as a current crowding area. However, as can be seen in Figure 2, the current flow does not pass through solder #6. Therefore EM cannot happen in solder #6. TM dominates the mass transport process (TM only) in solder joint #6. In solder #7, current enters the solder joint from the copper trace in the base, passes through the solder ball, and flows out through the aluminum trace on the crown. The electrons move in the opposite direction to the current. Considering the downward temperature gradient, we conclude that the overall effect in solder #7 is the

superimposition of TM and EM in the downward direction (TM + EM). In solder #10, current flows from the top to the bottom. The electron flow results in an electron wind force which is pushing mass upward. At the same time, thermal gradient drives atoms from top to bottom. Hence, solder #10 experiences TM and EM in the opposite directions (TM – EM).

From Figure 3 we see that solder #7 is the critical component in the entire test vehicle. When solder #7 fails ( $D = D_{cr}$ ), the damage parameters in solder #6 and solder #10 are still far below failure criteria. The comparison of three solder balls show that although TM alone (solder #6) does not produce damage as fast as EM, it can slow down (solder #10) or hasten (solder #7) the EM process significantly, as seen in Figure 3.

By comparison of the simulated time to failure (TTF) in solder #7 at different levels of ambient temperature ( $-20, -30, -40$  and  $-50^{\circ}\text{C}$ ) with the experimental result, as is shown in Figure 4, we observe that the finite element simulation is a good match for the experimental results. It is obvious that below  $-30^{\circ}\text{C}$ , time to failure increases very

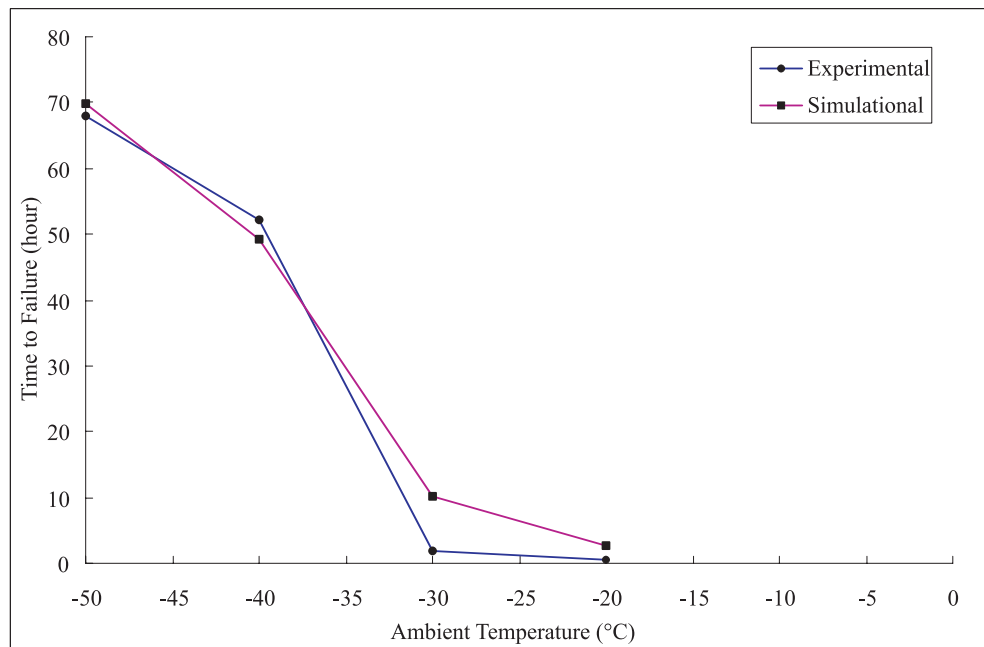


**Figure 4.** Comparison of experimental and simulation results

sharply. It is well known that TM and EM are diffusion-driven mechanisms. Hence, it is expected that lower temperatures result in a longer time to failure. However, a sharp increase in TTF below  $-30^{\circ}\text{C}$  needs to be studied further at the atomic scale by means of molecular dynamic simulations.

## 7. Conclusions

A fully coupled diffusion-mechanical-thermal-electrical damage model for simulating EM and TM-induced damage processes has been presented. The partial differential equation (PDE) forms of governing equations are discretized for FEM implementation. In this model, we have also embedded a coupled kinematic/isotropic hardening model with the flow rule from Tang and Basaran's [19] viscoplastic model for solder alloys, used to consider the viscoplastic behavior under high current density. The commercial FEM software ABAQUS is adapted to solve these PDE models by coding the user interface UEL and UMAT. This model provides a platform to simulate thermal field, electrical field, strain-stress field and diffusion progressing for solder joints and ULSI interconnects.

Based on this platform, a thermodynamics-based damage model is embedded to study the reliability of interconnections under service conditions. Using this code, simulations have been employed to investigate the damage evolution process under a series of complicated service conditions: TM only, TM + EM and TM – EM. The results

are compared with the experimental data to validate the model.

## 8. Acknowledgements

This research project has been sponsored by the US Navy Office of Naval Research Advanced Electrical Power Systems program, under the direction of T. Ericson.

## 9. References

- [1] Skaupy, F. 1914. Electrical Conduction in Metals. *Verband Deutscher Physikalischer Gesellschaften* 16, 156–157.
- [2] Seith, W. 1955. *Diffusion in Metallen; Platzwechselreaktionen*. Berlin: Springer-Verlag.
- [3] Wever, H. and W. Seith. 1955. New Results on the Electrolysis of Solid Metallic Phases. *Zeitschrift für Elektrochemie* 59, 942–946.
- [4] Ye, H., C. Basaran, and D. Hopkins. 2003. Thermomigration in Pb-Sn Solder Joints under Joule Heating During Electric Current Stressing. *Applied Physics Letters* 82(7), 1045–1047.
- [5] Ru, C.Q. 2000. Thermomigration as a Driving Force for Instability of Electromigration Induced Mass Transport in Interconnect Lines. *Journal of Materials Science* 35(22), 5575–5580.
- [6] Dan, Y., B. Y. Wu, Y. C. Chan, and K. N. Tu. 2007. Microstructural Evolution and Atomic Transport by Thermomigration in Eutectic Tin-Lead Flip Chip Solder Joints. *Journal of Applied Physics* 102(4), 043502, 1–6.
- [7] Chuang, Y.C. and C.Y. Liu. 2006. Thermomigration in Eutectic Snpb Alloy. *Applied Physics Letters* 88(17), 174105-3, 1–3.
- [8] Abdulhamid, M. and C. Basaran. In press. Influence of Thermomigration on Lead-Free Solder Joint Mechanical Properties. *ASME Journal of Electronic Packaging* [In press].

- [9] Shatzkes, M. and Y. Huang. 1993. Characteristic Length and Time in Electromigration. *Journal of Applied Physics* 74(11), 6609–6614.
- [10] Tu, K.N. 1992. Electromigration in Stressed Thin Films. *Physical Review B* 45(3), 1409–1413.
- [11] Blech, I.A. and C. Herring. 1976. Stress Generation by Electromigration. *Applied Physics Letters* 29(3), 131–133.
- [12] Blech, I.A. 1984. Stress Effects in Electromigration. *Journal of the Electrochemical Society* 131(8), 325C–325C.
- [13] Blech, I.A. and K.L. Tai. 1977. Measurement of Stress Gradients Generated by Electromigration. *Applied Physics Letters* 30(8), 387–389.
- [14] Blech, I.A. 1998. Diffusional Back Flows During Electromigration. *Acta Materialia* 46(11), 3717–3723.
- [15] Kirchheim, R. 1992. Stress and Electromigration in Al-Lines of Integrated-Circuits. *Acta Metallurgica et Materialia* 40(2), 309–323.
- [16] Bassman, L.C. 1999. Modeling of Stress-Mediated Self-Diffusion in Polycrystalline Solids. Ph.D. Thesis, Stanford University, 134 pages.
- [17] Blech, I.A. 1976. Electromigration in Thin Aluminum Films on Titanium Nitride. *Journal of Applied Physics* 47(4), 1203–1208.
- [18] Basaran, C., M. Lin, and H. Ye. 2003. A Thermodynamic Model for Electrical Current Induced Damage. *International Journal of Solids and Structures* 40(26), 7315–7327.
- [19] Tang, H. and C. Basaran. 2003. A Damage Mechanics-Based Fatigue Life Prediction Model for Solder Joints. *Journal of Electronic Packaging* 125(1), 120–125.
- [20] Lin, M. and C. Basaran. 2005. Electromigration Induced Stress Analysis Using Fully Coupled Mechanical-Diffusion Equations with Nonlinear Material Properties. *Computational Materials Science* 34(1), 82–98.
- [21] Sarychev, M.E., Zhitnikov, Yu.V., Borucki, L., Liu, C.L., and T.M. Makhviladze. 1999. General Model for Mechanical Stress Evolution During Electromigration. *Journal of Applied Physics* 86(6), 3068–3075.
- [22] Basaran, C. and C. Yan. 1998. A Thermodynamic Framework for Damage Mechanics of Solder Joints. *Journal of Electronic Packaging* 120, 379–384.
- [23] Gomez, J. and C. Basaran. 2005. A Thermodynamics Based Damage Mechanics Constitutive Model for Low Cycle Fatigue Analysis of Microelectronics Solder Joints Incorporating Size Effects. *International Journal of Solids and Structures* 42(13), 3744–3772.
- [24] Tang, H. and C. Basaran, C. 2001. Influence of Microstructure Coarsening on Thermomechanical Fatigue Behavior of Pb/Sn Eutectic Solder Joints. *International Journal of Damage Mechanics* 10(3), 235–255.
- [25] Basaran, C and S. Nie. 2004. An Irreversible Thermodynamic Theory for Damage Mechanics of Solids. *International Journal of Damage Mechanics* 13(3), 205–224.
- [26] Lemaitre, J.P. and J.-L. Chaboche. 1990. *Mechanics of Solid Materials*. Cambridge: Cambridge University Press.
- [27] Siewert, T., S. Liu, D.R. Smith, and J.C. Madeni. 2002. Properties of Lead-Free Solders. <http://www.williams-adv.com/packagingMaterials/lead-free-solder.php>.
- [28] Chung, C.M. and K.L. Lin. 2003. Effect of Microelements Addition on the Interfacial Reaction between Sn-Ag-Cu Solders and the Cu Substrate. *Journal of Electronic Materials* 32(12), 1426–1431.
- [29] Ye, H., C. Basaran, and D.C. Hopkins. 2004. Deformation of Microelectronic Solder Joints Under Current Stressing and Numerical Simulation: I. *International Journal of Solids and Structures* 41, 4939–4958.
- [30] Basaran, C. and M. Lin. 2007. Electromigration Induced Strain Field Simulations for Nanoelectronics Lead-Free Solder Joints. *International Journal of Solids and Structures* 44, 4909–4924.